Chem Soc Rev

TUTORIAL REVIEW

View Article Online
View Journal | View Issue

Cite this: *Chem. Soc. Rev.*, 2016, **45**, 1581

Fundamentals and applications of self-assembled plasmonic nanoparticles at interfaces

Joshua B. Edel,*[a] Alexei A. Kornyshev,*[a] Anthony R. Kucernak[a] and Michael Urbakh[b]

Received 23rd July 2015

DOI: 10.1039/c5cs00576k

www.rsc.org/chemsocrev

This tutorial review will introduce and explore fundamental and applied aspects of electrolytic interfaces incorporating nanoscale building blocks for use in novel applications such as sensors and tunable optics. In order to do this, it is important to understand the principles behind even the simplest of immiscible interfaces such as those of the liquid|liquid and solid|liquid. Qualitatively, the picture is simple however the complexity is easily compounded by the addition of electrolyte, and further compounded by the addition of more complex entities such as nanoparticles. Nevertheless combining all these components surprisingly results in an elegant solution, where the nanoparticles have the ability to self-assemble at the interface with a high level of control. Importantly, this opens up the door to the development of new types of materials with a range of applications which have only recently been exploited. Initially we begin with a description of the fundamentals related to liquid|liquid and solid|liquid interfaces both with and without electrolyte. The discussion then shifts to a description of biasing the interface by the application of an electric field. This is followed by an exploration of nanoparticle assembly and disassembly at the interface by controlling parameters such as ligand composition, charge, pH, and electric field. Finally a description of the state-of-the-art is given in terms of current applications and possible future directions. It is perhaps fair to say that these new frontiers have caused great excitement within the sensing community not only due to the simplicity of the technique but also due to the unprecedented levels of sensitivity and control.

Key learning points
(1) Gain understanding of the principles behind immiscible interfaces such as those of liquid|liquid and solid|liquid
(2) How and why do nanoparticles self-assemble at interfaces?
(3) How can nanoparticles be motivated to assemble and disassemble from the interface?
(4) What are the possible applications?
(5) Experimental and characterization challenges

Modern-day nanoplasmonics builds on many achievements both past and present, which have resulted in the development of novel platforms and methods for use in chemical analysis, electronics, and optics. In many cases, the end product can at times be either costly to fabricate or are technologically demanding. Recently there has been a glimpse of hope for an alternative strategy alleviating the complexities especially in the context of fabrication. This direction relates back to the dream of alchemists: find the magic composition and let the system build itself (Fig. 1). Whereas the ambitions of alchemists were to facilitate the self-assembly of not less than a 'homunculus', in nanoplasmonics we may have more modest dreams: the self-assembly of arrays of nanoparticles (NPs) delivering a unique optical response which can be used as novel analytical sensors or even tunable optical metamaterials. Coupled to this and above alchemy is the ambition of electrochemists, whose dream is to create adaptable tuneable systems near electrodes which can be controlled by applying a potential. In electrochemistry the potential drop is 'condensed' within nanometer dimensions of an electrical double layer in the electrolyte. Therefore, the application of 1 V could in principle be sufficient to dramatically change the assembly of structures at the electrodes. 1 V is not much in our everyday life, but electrochemists know how many events may occur within just 1 V and that they must apply it properly. Interestingly, in terms of the creation of novel self-assembled nanoplasmonic platforms, the alchemists'

[a] *Department of Chemistry, Imperial College London, SW7 2AZ London, UK. E-mail: Joshua.edel@imperial.ac.uk, a.kornyshev@imperial.ac.uk*
[b] *School of Chemistry, Tel-Aviv University, Tel-Aviv, 69978, Israel*

dreams have been realized, but the electrochemists' one has yet to be achieved. This article will provocatively discuss the main aspects of those achievements and challenges by first understanding the fundamentals followed by introducing new and exciting applications and developments.

Electrochemical interfaces

Perhaps the two most commonly used and relevant interfaces for controlling the optical response of NPs are either a liquid|liquid interface (LLI) of two immiscible electrolytic solutions (ITIESs) or a solid|liquid interface (SLI) using a (typically) transparent conducting film electrode with electrolytic solutions. In order to fully understand the working principles and complexity of such platforms, it is important to simplify and take a step back to obtain a clearer picture of the interface without NPs. The intention is not to give a detailed historical overview, as there are many excellent 'classical' reviews already available[1] and numerous others detailing the atomistic picture.[2] Instead, we present the reader with the most elementary features of an ITIES, as is shown in Fig. 2a, important for understanding the assembly of NPs. In the simplest form, an ITIES consists of an "oil" phase with large, low charge density,

Joshua B. Edel

Joshua Edel is a Reader within the Department of Chemistry at Imperial College London. In 2011 he was awarded a prestigious ERC Starting Grant on "Nanoporous Membranes for High Throughput Rare Event Bioanalysis". He works at the interface of chemistry, physics, and engineering on a wide spectrum of novel analytical methods related to improving detection limits over conventional techniques. Specifically, he specializes in the development of micro- and nano-scale devices for analytical and bio- analytical sensors, novel therapeutic strategies, ultra-high sensitivity optical and electrical detection techniques, diagnostics, and theranostics.

Alexei A. Kornyshev

Alexei Kornyshev holds a Chair of Chemical Physics at Imperial College. His long international career extended over Russia (1974–1992), Germany (1992–2002), and UK (since 2002): for details of the occupied posts, research achievements, publications, fellowships in learned societies/academies, awards and medals – see http://www.imperial.ac.uk/people/a.kornyshev. He is an expert in condensed matter theoretical chemical physics and its applications to electrochemistry, biophysics, nanoscience, and energy generation and storage. His current research interests focus on (i) DNA biophysics, (ii) ionic liquids and their applications for energy-harvesting and nanomechanics, (iii) direct and reverse electroactuation, (iv) molecular electronics and machines, and (v) optofluidics and nanophotonics.

Anthony R. Kucernak

Anthony Kucernak received his PhD on the "Photoelectrochemical study of passive films" (1991) at the University of Southampton. After a postdoc position (Cambridge, UK), he became a lecturer in Chemistry, Imperial College London (1995). He became a Professor of Chemical Physics in the same department in 2009. He is a deputy director of the Energy Futures Laboratory at Imperial. His research interest focuses on electrochemical systems including energy systems and liquid–liquid interfaces and the development of novel techniques to study such systems. He has coauthored over 100 publications in peer-reviewed journals and is a coinventor on more than ten patents. He is a winner of the 2006 Helmut Fisher medal.

Michael Urbakh

Michael Urbakh is an expert in theoretical condensed matter and chemical physics and their applications to electrochemistry, nanoscience, and biophysics. Through the years his particular areas of research were the optical properties of electrochemical interfaces, nanotribology, single molecule biophysics, electrowetting and nanophotonics. He has over 220 publications, 15 review articles, and filed several patents. He received his PhD in physics from the Moscow Physical Engineering University. From 1973 to 1990 he worked at the Frumkin Institute of Electrochemistry. In 1990 he moved to Tel Aviv University, where he is now a Professor at the School of Chemistry, Josef Kryss Chair in Chemistry at Surfaces and Interfaces and Head of the Sackler Institute for Biophysics.

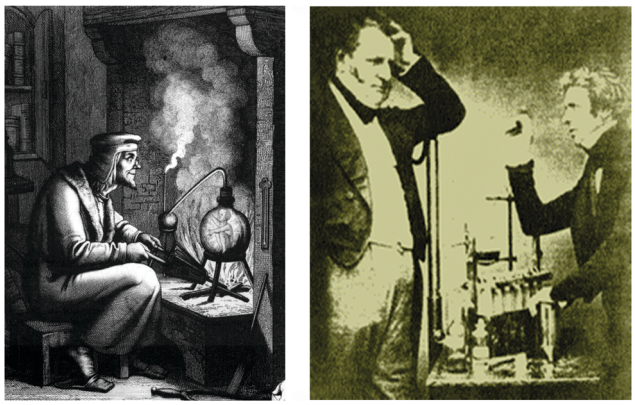

Fig. 1 Alchemists and electrochemists at work: different approaches. The right hand figure has been reproduced from Wikipedia commons by the Chemical Heritage Foundation.

hydrophobic organic ions and an aqueous phase with high charge density inorganic ions. Water and oil do not mix under ambient conditions. As a result an interface forms, which is known to be sharp even at atomistic scales but dynamically corrugated.[3] For instance, Fig. 3 shows a molecular dynamics simulation of the interface between water and nitrobenzene in which the interfacial region is <0.5 nm.

The two types of ionic species each prefer its own solvent phase and normally do not cross the interface. If they do, it will cost them typically an energy of ~ 0.5 eV per molecule for transfer. In other words if a tetrabutyl-ammonium cation, TBA^+, or tetraphenylborate anion, TPB^-, has to move from the bulk of dichloroethane to water, it will have to 'climb' some 0.5 eV up to the 'plateau' in the water phase; naturally at room temperature the population of such ions at the plateau will be negligible. The same is true if we want to move Li^+ or Cl^- from water to dichloroethane. This justifies the word immiscible in the name of the system: within a certain range of electrical potential drops across the interface, it is practically immiscible not only with respect to solvents but also the electrolytes involved. Hence this interface is often called a "liquid electrode". Let us polarize it, *i.e.* put it between two electrodes as shown schematically in Fig. 2b. Each electrode will be neutralized by the "electrical double layer", rich in counterions, resulting in two back-to-back double layers being formed at the LLI. Thus a large

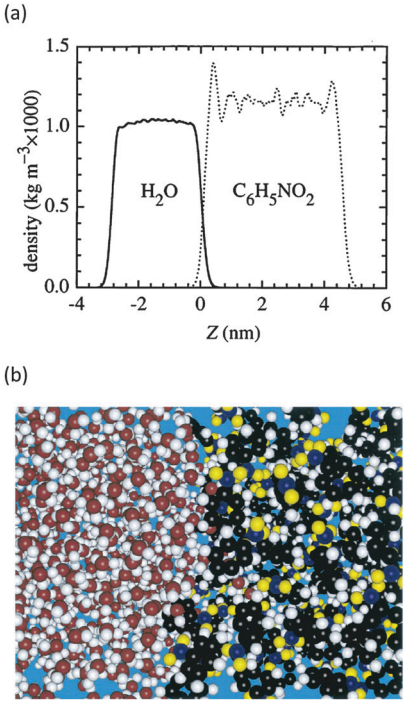

Fig. 3 Molecular dynamic simulations of an interface between water and nitrobenzene. (a) Room temperature density profiles of water and nitrobenzene. The liquid–liquid interface is around $Z = 0$. (b) A snapshot of the complete water (on the left)/nitrobenzene (on the right) simulation system. This figure has been reproduced from ref. 3 with permission from Elsevier.

portion of the overall voltage will drop across the interface, and will be distributed within the thickness of two back-to-back electrical double layers. The immiscibility of electrolytes may be jeopardized by applying too large a voltage across the interface such that the voltage will counterbalance the free energies of transfer between the two solvents. The range of voltages within which this does not occur is called an electrochemical window (EW). ITIESs have been shown to have EWs up to ~ 1.2 V.[4] Within this EW one can create large electric fields within the non-electroneutral region across the interface, for a relatively small overall applied voltage. Species that adsorb at the interface, *i.e.* behave like surfactants, may affect the distribution of potential at the interface, but will themselves experience that electric field. This in principle gives an opportunity to influence

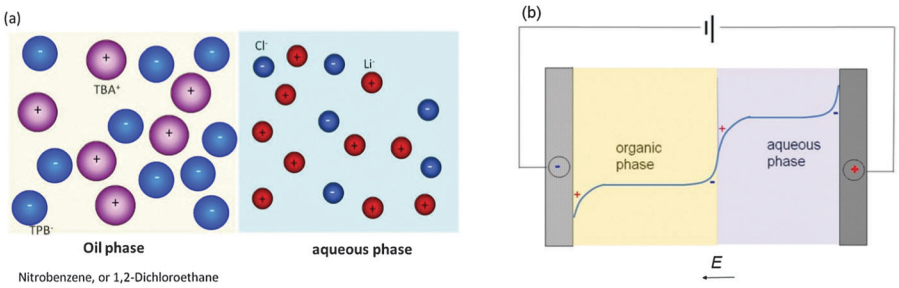

Fig. 2 (a) A cartoon of a typical ITIES at the molecular scale. The positive free energy of solvation of the ionic species in the neighbouring phase means that they do not spontaneously transfer into that phase. TBA^+ = tetrabutyl ammonium cation; TPB^- = tetraphenyl borate anion. (b) Polarised ITIES. The sign denotes the excess of cations (+) and anions (–) in the electrical double layers.

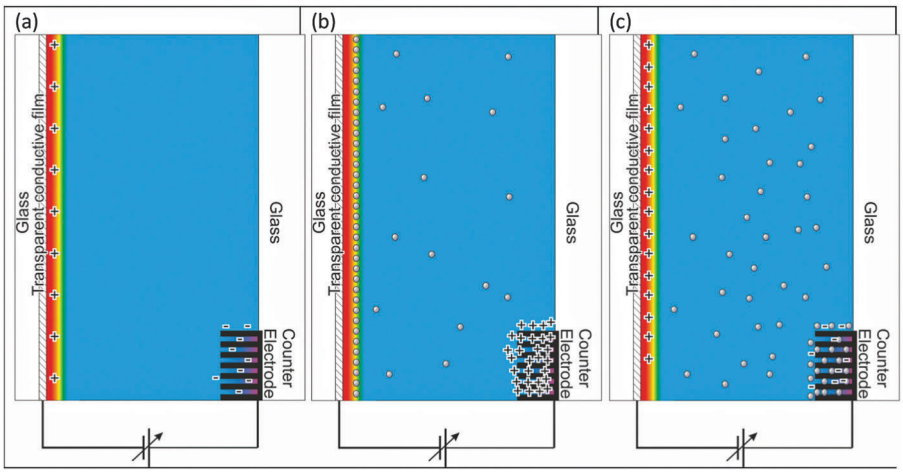

Fig. 4 Cartoon of a polarized transparent electrochemical cell involving a solid/liquid interface. (a) The double layers rich in cations forming on the negatively polarized transparent conducting film electrode and rich in anions on the positively charged high surface area counter electrode. (b) In the metal NP containing solution, the negatively charged particles are drawn to the positively charged transparent conducting film from the solution and at the same time positively charged ions build up on the counter electrode; (c) polarising the electrode negatively so that the nanoparticles are no longer stable at the interface leads to their dispersal throughout the solution and at the counter electrode. For simplicity, the negative charges on the NP are not shown, and neither are the free charges in solution.

the properties of the layers of any species that adsorb at the interface; if they are charged the position relative to the interface can be adjusted, or alternatively they can be removed from the interface.

A schematic of a SLI using a transparent conducting film (TCF) electrode is shown in Fig. 4. Transparent electrode materials may be formed using electrically conductive metal oxides such as fluorine doped tin oxide (FTO), antimony doped tin oxide (ATO), or tin-doped indium oxide (ITO). Adsorption of the species of interest is either spontaneous or if they are charged can be controlled by electrode polarization. The TCF surface can be protected by a self-assembled monolayer (SAM) film, to prevent the irreversible adsorption of the species of interest, and thereby facilitate a reversible control of adsorption–desorption of the species. TCFs also have their own EW but its meaning is entirely different. Whereas the EW for an ITIES is mainly limited by the onset of ion traffic across the interface and the discharge of the electrical double layers, at a solid electrode the discharge of the double layers is caused by the onset of the electrochemical, electron-transfer reactions of ions of electrolytes or of the solvent molecules (*e.g.* electrolysis of water), or reaction of the TCF material itself. Non-aqueous solvents with dissolved hydrophobic ions, like the organic phase of an ITIES, will typically give a wider EW on the TCF. In order for an SLI system to function efficiently, the counter electrode needs to have a similar surface area to that of the TCF in order to accommodate all of the particles. This can be achieved by having a counter electrode with an increased roughness factor by suitable control of the surface morphology.

Addition of plasmonic nanoparticles

Before introducing what happens when NPs are added to the above described systems, we must remind the reader that uncharged NPs tend to agglomerate and fuse due to attractive van der Waals interactions. This was well known from Pickering emulsions, where the particles were usually much larger, being micron or submicron in size. This effect is particularly strong for metallic NPs due to a larger Hamaker constant.[5] Stabilization of such NPs can be achieved using charged ligands which can either be covalently bonded or simply physisorbed to the surface. Sperling *et al.* have produced an 'encyclopedia' of commonly used ligands.[6] The terminal groups, which face away from the particle and into the surrounding liquid, are typically acidic rendering the ligand negatively charged with the degree of dissociation being dependent on the pH of the solution. The size also affects the stability of NPs. Simply, the smaller their size, the smaller their volume, and the smaller the van der Waals attraction between them. At the same time, the maximum number of charged ligands that can be accommodated will decrease due to the lower surface area. Since the surface scales as 2/3 power of volume, repulsion will rapidly prevail over attraction, as the particle radius is decreased. It is therefore easy to build a stable solution of NPs simply by controlling the size, surface charge, and pH without the particles agglomerating.

Each and every NP would in principle like to come and adsorb to the ITIES as the high oil/water interfacial energy will be removed or 'blocked', as long as the surface energy of the blocked section is larger than the surface energy of the oil/functionalized NP + water/functionlized NP interfaces. As charged NPs will naturally repel each other, their spacing can be controlled as the electrostatic repulsion of NPs will be Debye-screened by the ionic atmospheres in either of the electrolytes. Once more NPs reach the interface with the intension of settling, the final average inter-particle distance is found for which the repulsion is still tolerated, because of the gained reduction of the system free energy due to the mentioned surface energies. Thus the density of NP arrays at the LLI are entirely

determined by the compromise between the strength of the attachment to the interface and the strength of the interparticle repulsion.

The main constituent factors that determine the potential well for particles to be trapped at the interface have been studied,[7] with the most important being the capillarity effect. Charged NPs would prefer to be in water rather than in oil, due to the stronger Born solvation: water has a higher static dielectric constant than oil. The well at the interface is likely to be separated by a barrier from the potential plateau in water.[7] To make the well less deep in a nonpolarised system one must reduce the oil|water interfacial tension, say, by adding a surfactant. In a polarized cell the well can be made less deep or even to disappear if one polarizes the water side positively relative to oil. Thus voltage tuning can in principle affect the position of NPs relative to the interface: upon polarizing the water-side more negatively the NPs will be pushed further towards the oil; polarize it more positively and the NPs will shift towards water or leave the interface entirely and diffuse into the bulk, depicted in Fig. 5 and taken from ref. 8.

Electrochemical LLIs and SLIs have one general thing in common: they contain electrolytes, and both are polarizable. However, they also have a number of differences, some of which are crucial for the self-assembly of NPs, particularly for plasmonic applications. ITIES, when polarized, forms two back to back electrical double layers, one in the organic phase and one in the aqueous phase. From a fundamental point of view it is not clear if the double layer in the organic phase can, strictly speaking, be described by the simple Gouy–Chapman theory, particularly for solvents with a low static dielectric constant, such as *e.g.* dichloroethane (dielectric constant $\approx$ 10). Indeed, the Bjerrum length in such liquid (the length at which two unit charges will interact with the energy equal to the thermal energy) is eight-times larger than in water and the effects of Coulomb correlations may be substantial. However, the measured capacitance of the interface is well described by the Vervey–Niessen theory, which is based on two back-to-back Gouy–Chapman double layers.

The capillary well for NPs assembled at an LLI may be several eV deep for large NPs. Electrostatic interactions of NPs at the interface will be screened by either electrolytes either in a linear fashion or if Coulomb correlations are important in some other, currently less known way. Since both phases are transparent to light, the plasmonic response of the array of NPs settled at the interface is essentially the response of the array. On the other hand, the driving forces for NPs to approach an electrode at a SLI, when the electrode is nonpolarized, are van der Waals attraction and image forces, but there is no capillary effect. This attraction will be the largest for metallic electrodes. To protect the electrode surface against the NP sticking to it, this may be covered by the self-assembled monolayer (SAM), *e.g.* short alkanes, silanised at one end building a chemical bond with the substrate. This will warrant 'soft landing' of NPs on the surface and their easy removal when the electrode is polarized with a charge of the same sign as the charge of the ligands attached to NPs (functionalization of the surface with SAMs may not be needed for graphene).

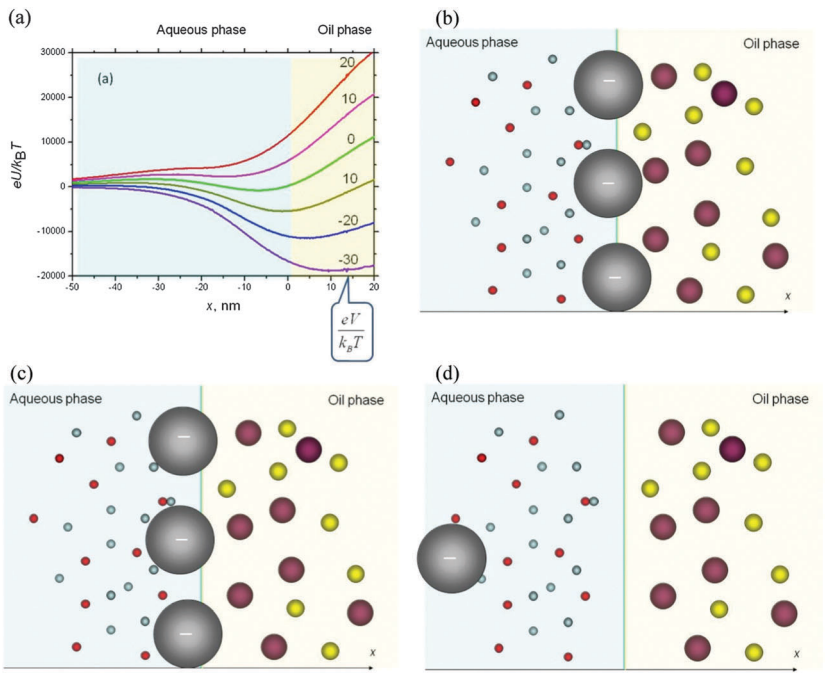

Fig. 5 Controlling the position of NPs with voltage. (a) Model calculations for 20 nm radius NPs, −1000*e* charge on them and in diluted electrolytes; *V* is defined as the potential difference between water and oil bulk – in the graph the water level is kept constant. (b) Putative position at the nonpolarized interface, eV/k_BT = 0; (c) polarizing oil more negatively, *e.g.* corresponding to the curve eV/k_BT = 10 the particle shifts further towards water (d) even further negative polarization of oil, *e.g.* eV/k_BT = 20, pushes NPs to water bulk; they are no longer trapped at the interface. This figure has been reproduced from ref. 8 with permission from the American Chemical Society.

Electrostatic interactions between charged NPs and the electrode–electrolyte interface and between the NPs at the interface will be different from those in ITIES. Similar to the ITIES, the Coulomb repulsion between NPs will be screened by the electrolyte, but on the electrode side of the interface the screening will be different for metal, semi-metal ITO, or graphene cases. Whereas the case of graphene has not been studied yet, for ITO and metal we know what to expect based on the theory of image forces and interionic interaction at such interfaces developed many years ago (for a review see ref. 9). The whole question of interactions that keeps NPs close to SLIs requires further investigation. More complicated effects of Donnan equilibrium and nonlinear interaction of charges of ligands with electrolyte ions may further modify the electrostatic interaction of NPs with each other and with the electrode.

Experimental methods to probe metallic nanoparticles at the LLI

A number of approaches are available for studying the presence of nanoparticles at liquid–liquid interfaces. There are added difficulties in trying to understand the positions of the particles relative to the interface and each other compared to the situation when they are at the more easily accessible air–liquid interface. The techniques used can be classified as real-space imaging techniques, reciprocal space imaging techniques, and indirect techniques which infer the presence of particles by looking at a change in some specific parameter.

Real space studies

Although individual particles much smaller than the optical resolution limit may be studied using optical techniques, such as total internal reflection fluorescence,[10] it is not possible to resolve particles in ensembles unless suitable super-resolution optical techniques are used. Currently such super resolution techniques have not been applied to nanoparticles at liquid–liquid interfaces, although high resolution images of 1–5 nm dodecanethiol-capped silver nanoparticles at a trichloroethylene-in-water droplet have been recorded using an environmental TEM under an atmosphere of 2–4 Torr water vapour.[11] An alternative to this approach is to use freeze-fracture cryo-SEM, which has been successfully used to image 100 nm gold particles at the water/*n*-decane interface and determine the contact angle of the particles at the interface.[12]

Reciprocal space studies

X-ray reflectivity and diffuse scattering of toluene–water LLI have been used to estimate the position of the gold nanoparticles from the interface during their formation and growth.[13] The electron density profile of these clusters determined by X-ray reflectivity exhibits three layers of nanoparticles as a function of depth which evolves with time while diffuse scattering data imply a strong reduction in interfacial tension.[13] By making measurements in a Langmuir trough, Kubowicz *et al.* were able to measure the surface pressure-area for 1.1 nm radius gold particles at the *n*-tetradecane/water interface whilst simultaneously measuring X-ray reflectivity and grazing incidence X-ray diffraction.[14]

Other studies

A review of spectroscopic studies of molecular interaction at the liquid–liquid interface using IR, UV-visible, Raman, fluorescence spectrophotometry, and optical 2nd order techniques is provided by Perera *et al.*[15] with some of the techniques already being applied to systems composed of nanoparticles at the LLI. For instance SERS[16,17] and optical second harmonic generation[18] can in principle be used to measure the assembly of particles at the surface. The presence of particles at the interface has a significant effect on the capacitance of that interface, and such studies maybe used to also follow nanoparticle adsorption.[19] A more direct measure of the interparticle separation and particle position relative to the interface can be determined from localized surface plasmon resonance (LSPR).[20] Angle and wavelength resolved optical reflectivity experiments utilising 60 nm gold particles at the [heptane + DCE]/water interface[21] show significant effects of surface coverage, as expected from theory. Interfacial tension of 200 nm Ag particles at the water decane interface can be measured through pendent drop tensiometry.[22]

How do we know that nanoparticles are at the interface? Do they form a monolayer?

At first glance there is not much reason to expect NPs to form multilayers at the interface. The main driving force for the NPs to come to the interface is to pierce and thereby block it. Such a simple argument will suggest that without this effect, there would be no impetus for charged NPs to come close to the interface.[8,23,24] As explained above, its energy is lower in water due to stronger Born solvation. However, the situation is in fact more complicated, as will be discussed below. Multilayer NP formation may result from the reduction of Coulomb repulsion between NPs just below the limit at which the particles can agglomerate. This may occur due to (i) a reduction of ligand charges on the NPs *via* acid–base chemistry, (ii) decrease of ligand density on the NPs, and (iii) increase of the bulk electrolyte concentration to screen electrostatic interactions. Agglomeration at the interface may occur earlier than in the bulk due to a collective effect: once the first hexagonal layer of NPs forms at the interface, it may 'catalyze' the adhesion of the next layer. This would require a subtle balance of several system parameters, including taking into account the Donnan equilibrium.

On which side of the interface do the nanoparticles sit?

This is a question that has been a matter of debate ever since the realization that NPs can assemble at a LLI. A possible route towards obtaining a clearer picture would be to measure the

contact angle in a three phase system: organic droplets in the aqueous phase on an atomically flat gold surface. Although one cannot literally transfer the results of such experiments on what will happen with NPs at the ITIES, one would still expect that if the contact angle is close to 90°, a round NP will tend to sit halfway between the oil and aqueous phase. A more acute angle would imply that the gold surface is more hydrophobic, as a result the NPs would penetrate deeper into the oil phase. The contact angle and the overall effect are expected to be influenced by the concentration of electrolytes on either side of the interface and definitely by the type of functionalization of the metal surface. Recently Schlossman's group[25,26] came up with a nontrivial suggestion that the interaction of NPs with counterions on the oil side is very different from that on the aqueous side. In DCE, the dielectric constant is eight-times smaller than that of water, and Coulombic interactions between single charges would have a similar effect to Coulombic interactions between triple charges in the aqueous phase. They supported these arguments by molecular dynamics simulations (performed for small, 2 nm NPs), and X-ray reflectivity experiments which we will discuss in more detail below: the upshot of those studies was that their NPs, functionalized by positively charged ligands, are predominantly shifted to the oil side due to strong Coulomb coupling with the organic anions, Fig. 6.

Localization of nanoparticles at interfaces and plasmonic applications

Once the NPs gather in a dense monolayer at the interface, they can perform two different functions. First they can be used as plasmonic antennas, creating hot spots for electromagnetic radiation in between the NPs. This in turn can be used for applications such as Raman spectroscopy where an analyte molecule gets captured in the hot spots resulting in its Raman fingerprint being significantly enhanced. Raman scattering scales roughly proportionally to the 4th power of the electric field, and thus the enhancement of electromagnetic radiation in hot spots dramatically amplifies Raman scattering, in a fashion similar to SERS (surface enhanced Raman scattering) on rough or nanostructured metallic surfaces, where the plasmon resonance effect is utilized. In an array of metallic NPs we deal with coupled localized plasma oscillations, excited by light in each NP. A further interesting application relates to the reflection of light induced by the formation of a dense layer of NPs assembled at either a LLI or SLI. For this, one needs sufficient electronic mass, *i.e.* NPs must be large enough, typically about 20 nm in radius or larger. Clearly, if one could sufficiently vary the population of NPs at the interface by the application of a voltage, one would create an electrovariable mirror.[7]

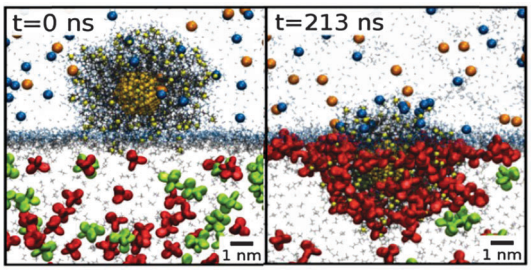

Fig. 6 Snapshots for molecular dynamics simulations that illustrate a small NP consisting of a 2 nm gold core coated with ~100 positively charged trimethylammonium-terminated ligands (TTMA Au NP) at the interface between a 5 mM NaCl aqueous phase (top) and a 5 mM $BTPPA^+TPFB^-$ 1,2-dichloroethane (DCE) phase (bottom). At the beginning of the simulation (t = 0 ns), the chloride ions form a diffuse cloud above the NP in the aqueous phase, but at a later time (t = 213 ns) $TPFB^-$ ions condense onto the NP as it submerges into the lower permittivity phase, DCE. The results of the X-ray experiments, which will be discussed later, suggest that NPs functionalized with these ligands are submerged even slightly deeper into the DCE phase than observed in the MD simulations, though the NPs remain in contact with the aqueous phase. This figure has been reproduced from ref. 25 with permission from the American Chemical Society.

Localization of metallic NPs in ITIES was first demonstrated by the groups of Schiffrin[27] and Girault,[28] albeit using small NPs with diameters less than 2 nm. The voltage-induced assembly of mercaptosuccinic acid-stabilized Au NPs with a diameter of 1.5 ± 0.4 nm has been demonstrated at the water|1,2-dichloroethane interface of ITIES.[28] For small particles, voltage-controlled reversibility of adsorption–desorption has been achieved. However, increasing the NP size poses a significant challenge as the depth of the capillary well is proportional to the square of the NP radius with the proportionality prefactor being determined by interfacial tension at an LLI (*cf.* an approximate formula A2 in ref. 7). Electrostatic interaction of NPs with the electric field in the electrical double is roughly proportional to the number of charges on the functionalized NP, *i.e.* it also scales with the square of the NP radius. But it also grows with the applied voltage. For large NPs, the 'capillary trapping force' at the interface is orders of magnitude greater than for small NPs, but so will also be the electrostatic force. For a sufficiently large voltage across the ITIES the electrostatic interaction may compete with the capillary well: suitable polarization of the interface may eliminate the well (*cf.* Fig. 5a and ref. 7 and 8). However, for this to occur, a fine balance must be achieved. To be able to move the particle away from the interface (back into the water) we need to maximize the electric field acting on the charges of the ligands, and if possible, minimize the interfacial tension (by using mixed solvents). Achieving this will mean achieving reversibility of potential controlled adsorption–desorption of NPs, but for large NPs it is a challenging task.

The presence of NPs at the interface has been quantified by measuring the electrochemical admittance and quasi-elastic laser scattering (QELS), with both techniques suggesting that the surface concentration of the NPs at the LLI is reversibly controlled by the applied bias potential.[28] The analysis of the electrocapillary curves constructed from the dependence of the frequency of the capillary waves on the applied potential and bulk particle concentration gave even more quantitative information, indicating that the maximum particle surface density

is 3.8×10^{13} cm^{-2}, which corresponds to about 0.6 (60%) coverage of the surface for the 1.5 nm diameter particles.

Much larger Au/Ag core–shell NPs ranging between 16 and 20 nm in diameter have also been studied.[18] Whereas citrate stabilized Au NPs in that range showed clear agglomeration and multilayer formation at the interface, the core shell NPs were able to achieve four times higher charges on a silver shell. This higher charge density likely resulted in Coulomb repulsion prevailing over van der Waals attraction. Information on their reversible voltage-controlled presence on the surface was obtained *via* second harmonic generation (SHG) as well as UV-vis spectroscopy. However, the density of the layer was not determined. Although it was clearly shown that a systematic increase of electrolyte concentration causes the agglomeration of NPs.

Later, the Girault group have performed capacitance measurements of a polarised ITIES and showed that the capacitance of the interface increases in the presence of an adsorbed monolayer of citrate-coated gold NPs,[19] which the authors related to an increase of the interfacial charge density or an increase of the interfacial corrugation. This observation has been rationalized in a follow up theoretical paper by Marinescu *et al.*[29] where it was shown that the interfacial capacitance can bear clear signatures of adsorption of NPs to it, if compared with the data for a bare interface. However, quantitative characterization of the structure or even density of the layer is not straightforward.

When an SLI is used, there may not be such strong driving forces for NPs to be adsorbed at nonpolarized electrodes as in ITIES. Although there will be van der Waals and image charge attraction forces acting between the NPs and the solid surface, these effects are unlikely to be significant. Estimates, based on a classical Lifshitz type formula using 20 nm radius Au NPs, and ITO show that the potential well due to van der Waals attraction cannot compete with the electrostatic repulsion between the similarly charged electrode surface and NPs. This implies that the NPs could be removed from the surface by sufficient polarization of the electrode within the EW. Multilayers of NPs may form at the interface when NPs are drawn to the surface by the polarization of the electrode of a sign opposite to the sign of the charge on NPs. But the most important issue then is, if such layers are formed, would they be removable from the SLI surface by reversing the electrode polarization.

'Yes' or 'no'? A medieval style experiment

If one suspends NPs in an aqueous solution at a concentration that is sufficient to just cover the interface, then the solution will look slightly rosy. Deposition of the particles at the interface leads to a transparent solution. As the NP concentration in bulk solution can easily be determined using UV-vis spectroscopy, it is possible to approximate the number of NPs assembled at a LLI or even SLI simply by comparing the bulk concentration before and after the assembly. Such experiments have recently been reported[20] using 16 nm diameter Au NPs stabilized with the ligand 12-mercaptododecanoic acid (MDDA). The –SH group of the ligand binds to the Au surface whilst the 12 chain carbon and the acid termination ensure that the NPs will not aggregate at the interface. Furthermore adsorption and desorption from the interface can simply be achieved by varying the pH (or acidity of the solution) which directly affects the net negative charge on the ligands, Fig. 7. As the total charge decreases the NPs will desorb from the interface. Therefore a 'quasi'-reversible effect can be obtained albeit by ''chemical modulation'' rather than electrochemical modulation. One can imagine that a combination of chemical and electrochemical modulation can be used to fine tune the adsorption/desorption forces especially when working with larger particles.

Shift of the plasmon resonance – tuning the optical properties

Stepping away from medieval style experimentation where particles are simply adsorbed and desorbed from the interface, more sophisticated experiments can be performed to precisely control the density of NPs assembled. Theory suggests that the plasmon resonance shifts to the red as the inter-particle

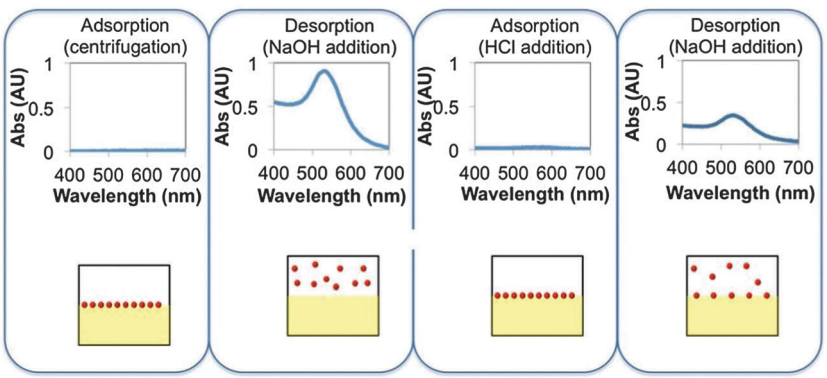

Fig. 7 Adsorption and desorption of gold NPs from the aqueous electrolyte/1,2-dichlorethane interface induced by varying the charge on NPs *via* varying the acidity of aqueous solution. This figure has been reproduced from ref. 19 with permission from the American Chemical Society.

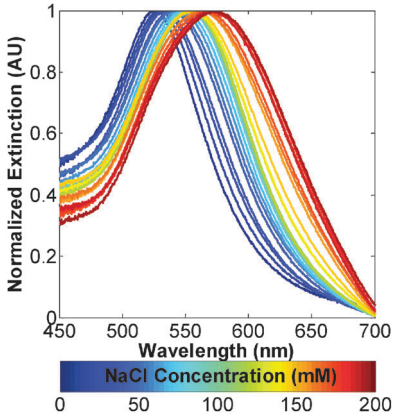

Fig. 8 Observation of the change in the density of NPs at the liquid–liquid interface with the increased screening of Coulomb repulsions between them. This figure has been reproduced from ref. 19 with permission from the American Chemical Society.

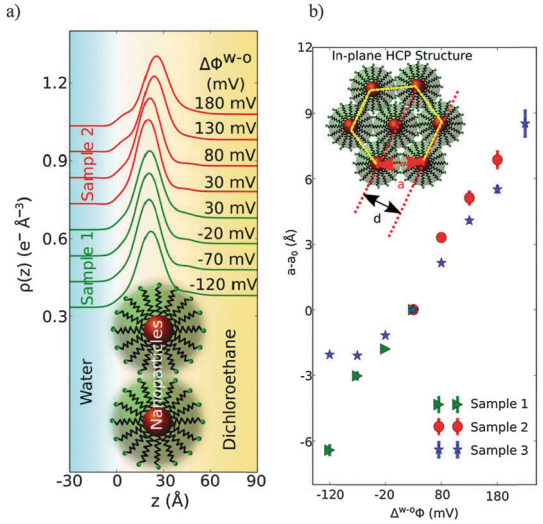

Fig. 9 (a) Electron density profiles of TTMA-functionalized Au NPs in the water|DCE ITIES. Variation of electron density $\rho(z)$ along the direction z (perpendicular to the interface) is obtained by fitting X-ray reflectivity data. A cartoon of NPs at the interface is also shown. The peak in the electron density profiles indicates the location of the NP gold core. The profiles demonstrate that TTMA-functionalized Au NPs are located primarily on the DCE side of the interface with small changes in their depth as the electric potential difference $\Delta\phi^{w-o}$ across the interface is varied from −120 mV to +180 mV. (b) Electrovariable lattice spacing of a 2-dimensional NP array formed in the water|DCE ITIES.[25] The variation in the nearest-neighbour spacing a, measured by grazing-incidence X-ray diffraction, is shown for three different samples as a function of the electric potential difference across the interface, $\Delta\phi^{w-o}$. The spacing a is referenced to the spacing a_o measured at $\Delta\phi^{w-o}$ = 30 mV for each sample (a_o = 67.2, 61.5 and 64.5 Å for samples 1, 2 and 3, respectively). Inset: cartoon of the 2D hexagonal close-packed structure of NPs illustrating the nearest-neighbour spacing a and lattice spacing d. This figure has been reproduced from ref. 25 with permission from the American Chemical Society.

separation decreases, and this is what has been observed experimentally,[20] *cf.* Fig. 8. The distance between NPs has been varied by changing the concentration of the electrolyte in the aqueous phase, which affects the screening of Coulombic repulsion between NPs. For example, the Debye screening length for a 1 mM and 100 mM solution is approximately 10 and 1 nm, respectively. Such a variation in inter-NP distances leads to a plasmon resonance shift of ~50 nm, making this method exceptionally sensitive to tuning the optical properties.[30] Equally, the electrical polarization of the cell which increases NP's propensity to settle at the interface will favour higher density of NPs at the ITIES, also producing the red shift.

Direct observation: *in situ* X-ray diffraction and SAXS

Schlossman's group[25] has studied both X-ray reflectivity (at 10^{-2}–10^{-5} radian angles) and grazing-incidence small-angle X-ray scattering on arrays of small 2 nm NPs assembled in a water|DCE ITIES. The NPs were functionalized with trimethylammonium-terminated ligands which are positively charged and 2 nm in length and not affected by pH. The NPs were shown to form a hexagonal array along the interface. The lattice constant of the array, *i.e.* the centre to centre separation, was 6–7 nm, *i.e.* the functionalised particles were almost in close contact. There are some domains with bare interfaces in between (the area of the LLI covered by NPs was about 80 percent), but within the domains of NPs the order is close to a perfect one. Interestingly the NPs were shown to be almost completely immersed in the DCE side (Fig. 9a) and could be electrovariably controlled, Fig. 9b. For example, it was shown that the lattice spacing of the array could be tuned by applying an appropriate voltage across the interface.

As mentioned above, the authors explain the shift of NPs to the oil side of the interface to be due to strong coupling of NPs with the anions in the organic phase (*i.e.* there is an eight-fold increase in Coulombic interaction when compared to the interaction between NPs and anions in the aqueous phase). This effect is known under the name of strong Coulomb correlations. These are responsible for the effect of the like charge attraction, found in colloid systems with a large Bjerrum length.[31] This effect could keep NPs at the DCE side of the interface, as supported by specially performed MD simulations.

It should be noted that the position of NPs at the interface may be different for acidic ligands as they will likely have a weaker propensity to dissociate on the oil side of the interface. If this is true, the nonlinear coupling with organic anions may not occur and the particle will be shifted more towards the aqueous side of the interface. Indications that this has been the case have been observed indirectly *via* performing SERS,[16] where a lower signal was observed when analytes were initially dissolved in the oil phase as opposed to the aqueous phase. Ultimately X-ray experiments would have to be performed to validate if this hypothesis is indeed correct by varying the ligands, electrolytes, the NP size and solvent. Solvent effects will be of special interest, as Coulomb correlations and charge attraction can be tuned. For example such effects are expected

to be negligible if nitrobenzene is used as the dielectric constant is only 2.5 times smaller than that of water.

Recently synchrotron X-ray experiments for ITIES with much larger NPs and functionalized with negatively charged mercaptododecanoic acid at different electrolyte concentrations have been performed at the Diamond Light Source by the Velleman *et al.* (to be published). Preliminary results confirm that hexagonal arrays are formed at the interface with tuneable lattice constants ranging between 20 and 40 nm simply by controlling the ionic strength. The results are qualitatively consistent with a plasmonic ruler.[20]

Is there an ideal nanoparticle size?

We now have sufficient confidence that proper control of the net charge of NPs and the strength of their screened Coulomb repulsion can provide monolayer arrays of NPs at the LLI. Similar studies for the TCF electrode configurations are in progress. Now comes the question, what will be the preferable size of NPs for different applications?

Can we use such arrays as antennas and mirrors? For optical applications, small NPs, of about 2 nm, will not be of much use. For SERS the probe volume of the hot spots will be very small, for mirrors – reflectivity will be miserable, practically nonexistent (see below). For particles of 43 nm in diameter, remarkable results for SERS detection have been obtained. For mirrors we require NPs with diameter 40 nm and higher.

SERS at liquid|liquid interfaces

Recently there has been much interest in tailoring NPs adsorbed to an ITIES for use in SERS based applications. The motivation arises from the possibility of improved performance and simultaneous multiphase detection. Furthermore, as counter-ions will want to accumulate near the charged nanoparticles, such a system is ideal for capturing analytes. An example is shown in Fig. 10 where SERS detection has been shown for analytes such as 2-mercapto-5-nitrobenzimidazole (MNBI) dissolved in the aqueous phase and 4-methoxy-α-toluenethiol (MATT) dissolved in the organic phase.[16] This was performed using citrate stabilized 40 nm diameter NPs. The limit of detection in the case of MNBI is much lower than for MATT, *i.e.* the SERS signal of the former is much higher.

What stands behind this difference? The most simple (perhaps naïve?) point of view would be to assume that weaker or no ionization of acidic groups in the oil side results in NPs correspondingly being shifted to the aqueous phase. Hence the hydrophobic molecules will be on average farther from the hot spots than the hydrophilic molecules, resulting in a lower SERS signal. At a first glance, it appears to contradict Schlossman's conclusion[25] that the position of NPs is shifted towards the oil phase, which in their case was attributed to strong, nonlinear interaction with ions dissolved in the organic phase. However, there could be another factor that can explain this difference (proposed by Ron Grill of the University of Twente). SERS signals

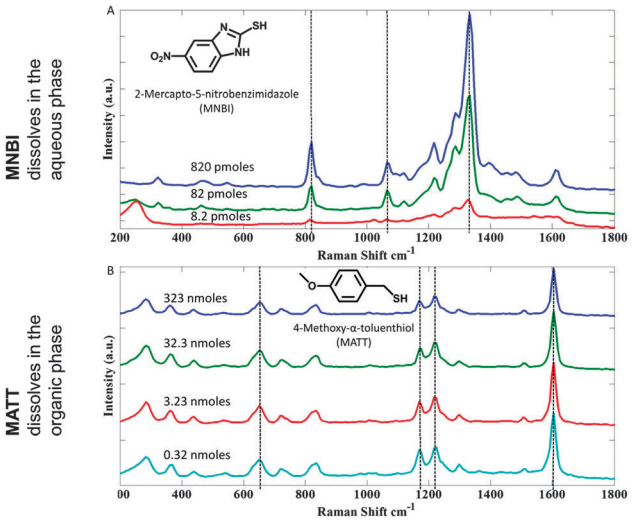

Fig. 10 SERS dilution series for analytes dissolvable in different phases. The amount of analyte is given per 1 mL of water or oil, correspondingly. This figure has been edited from ref. 16 with permission from Nature Publishing Group.

are sensitive to the orientation of analyte molecules relative to the vector of the electric field. For the normal incidence of light, this vector lies parallel to the interface. Amphiphilic but still strongly hydrophobic MNBI is likely to be oriented perpendicular to the interface, to immerse their 'fatty bodies' into the oil, and that may influence the orientation of their dipole active groups. In contrast, MATT molecules, having stronger hydrophilic groups, are likely to lie more parallel to the interface which may result in amplified Raman signals.

To verify this interpretation, one must perform molecular dynamic simulations, which could demonstrate the orientation of these analytes and their induced dipole moments relative to the interface. In addition it will be important to perform the same kind of measurement as in ref. 16 in the presence of organic electrolytes. Note, that the orientation of molecules may be further complicated by the density of the NPs, which could result in constraints on the accommodation of analytes in the hot spots. This factor should, however, be less stringent when the size of NPs is much greater than the size of the analyte molecules, as there will always be a room to accommodate such analytes in their preferred orientations in the voids between the NPs. Generally many analyte molecules get into the hot spots affecting the signal but only in linear proportion to their amount; thus the amplification of the Raman signal due to the nonlinear effect is a much more important factor for the trace analyte detection.

Generally, the signals recorded indicate relatively dense packing of NPs at the LLI, although this fact itself cannot guarantee that they form a monolayer. It should be noted that these results were obtained using citrate stabilized particles and not mercaptanes as used for the plasmonic ruler. The latter are chemically bound to NPs and presumably deliver larger average charges than citrates. Enhanced Coulomb repulsion between the NPs may not allow them to come close enough to

each other and the hot spots are not sufficiently 'hot'. Note that for mercaptane-functionalized NP assemblies, their submonolayer structure at the interface is understood. Whereas aggregation and island formation cannot be excluded for citrate stabilized assemblies. Recently Dryfe and colleagues have built on this platform by successfully performing the electrochemical manipulation of SERS-active small silver NPs at an aqueous|DCE interface. They were able to quantify the adsorption and desorption simply by monitoring the Raman spectra.[32] The same group also performed complementary measurements by functionalizing graphene with NPs at an oil|water interface and monitoring it using Raman spectroscopy.[33]

An interesting recent development was in the creation of a novel platform for the detection of heavy metal ions in water, such as, *e.g.* Hg^{++}, indirectly through their attachment to Au NPs decorated with SERS active polyaromatic ligands (PALs).[34] It was found that upon addition of Hg^{++}, the SERS enhancement would increase 100 fold. Fig. 11a shows the full Raman spectrum for the two best performing PALs – 1,8-diaminonaphthalene (1,8 DAN) and 1-naphthalylamine (1NAP), in a pure electrolytic buffer solution and in the presence of 10^{-4} molar solution of $HgCl_2$ – a source of Hg^{++} ions. The nature of this enhancement has yet to be investigated. A speculative explanation of this effect is sketched in Fig. 11b where it is proposed that π-stacking of aromatic rings contributes to the NPs being linked *via* bridging of the mercury ion. Doing so decreases the spacing between the NPs and at the same time increases the field enhancement. Furthermore, the presence of $Hg^{++}Cl_2^-$ in the gap between the NPs, bridged by PALs to NPs, may cause excitations of some charge transfer modes that can add a 'chemical contribution'[35] to further enhance the Raman signal.

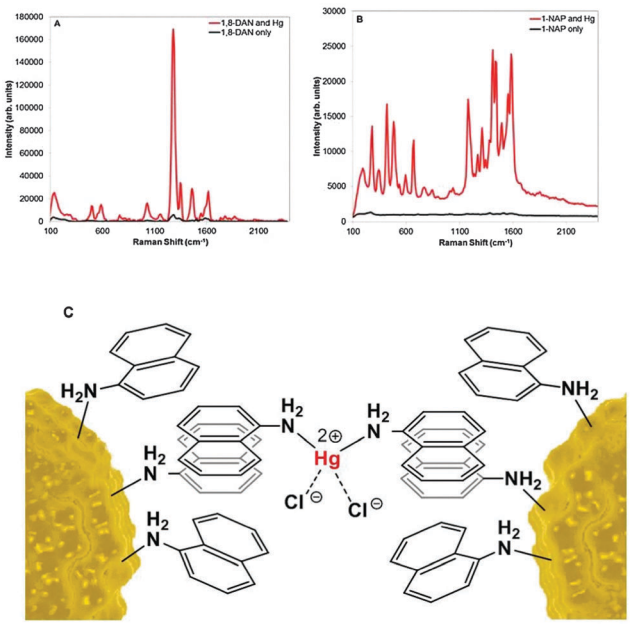

Fig. 11 Enhancement of the Raman signal of (A) 1,8 DAN and (B) 1-NAP ligands in the presence of 10^{-4} molar concentration of Hg^{++} ions. (C) A putative model for binding of 1-naphthylamine (1-NAP) to the NP surface and the complexing mechanism for Hg^{++} binding to outstanding free nitrogen terminals. This figure has been reproduced from ref. 34 with permission from Wiley.

A nanoplasmonic mirror

An exciting prospect of working with NPs in ITIES is that they can form wavelength specific reflective metallic sheets depending on the NP size and lattice constant. This opens the door to applications such as reversible and tuneable optics. Interestingly this area of research is a fine example of theory being developed in the first instance[8,36,37] with experimental results following suit. Perhaps somewhat surprising and counterintuitive a monolayer of Au NPs at an LLI or SLI can easily reach 80% reflectivity and extend over a broad frequency range. This level of reflection can be achieved for NPs that are 40 nm or larger and closely packed, with the average surface-to-surface separation between the NPs substantially smaller than half of their size. This effect is a result of the incident light exciting local plasmon modes inside the NPs. If the lattice constant of the NP arrays is relatively short, these modes result in 'bonding' and 'antibonding' eigen states,[38] working as antennas transmitting some part of the light, but also reflecting a large portion of it backwards. The reflection itself takes place because of the energy/wave number band-gap for the propagation of light, which is centered around the frequency of the localized plasmon. The width of the gap and its position depend on the material of NPs, their size, and coverage (*i.e.* average distances between the NPs).

There is always some absorption of light, due to the dissipation of localized plasmon modes in NPs,[39] including Landau-type dissipation in the metal bulk, electron–phonon scattering, and the effects of the nanoconfinement which gets stronger in smaller NPs. There is also transmission of light through the layer. The reflection is substantial when the light 'meets a sufficient electronic mass' and excites plasmons with substantial oscillator strength. The reflection spectrum is very different for s- and p-polarized light, and exhibits a strong angle dependence. The position of the reflection maximum can easily be manipulated by using core–shell NPs where the plasmon resonance can be tuned from the ultraviolet to the near-infrared regions of the visible spectrum.

Fig. 12 shows typical graphs that characterize reflection for an array of gold NPs at a DCE|aqueous interface. Displayed are the results of calculation using effective medium theory (EMT)[36] and the Drude–Lorentz approximation for the bulk dielectric constant of gold. EMT treats localized plasmon excitations in spherical NPs in the monolayer as coupled dipolar modes, with due account for image interactions of the 'dipoles' with each other and with their images, which should be present as optical dielectric constants of the two phases are different. Image forces are usually insignificant at an LLI but could play a dramatic role for NPs on solid electrodes.

In its nature, this EMT is a modification of an old theory of Persson and Liebsch[39] extended to an array positioned at the interface. Continuum in character, describing the layer of NPs as a film with an effective frequency-dependent dielectric

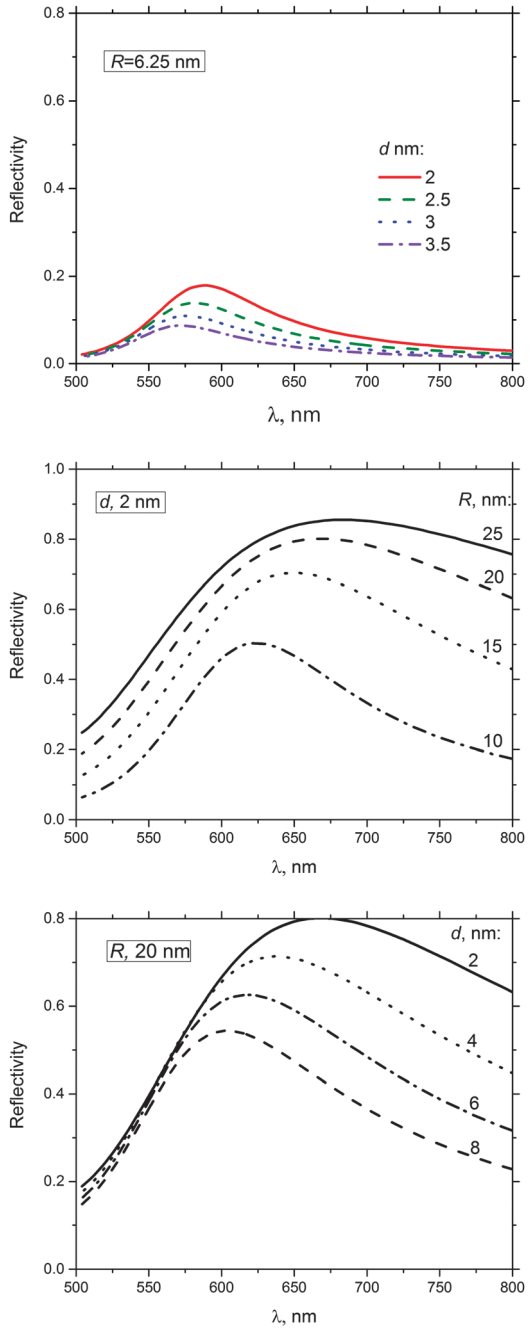

Fig. 12 Reflection from a hexagonally structured monolayer of gold NPs at the water/DCE interface (light propagating from the DCE side at normal incidence), calculated (specially for this article) following the Effective Medium Dipole Approximation Theory[36] and Drude–Lorentz approximation for the dielectric function of gold. The upper panel displays weak reflection from the layer of smaller sized NPs (of radius 6.25 nm) for indicated values of surface to surface separation, d. The middle panel shows the effect of the size of NPs for dense packing (d = 2). The lowest panel shows the effect of surface-to-surface separation for medium size NPs, R = 20 nm. The decrease of surface-to-surface separation moves maximum of reflection to the red.

function (which in turn is calculated, expressed through the frequency-dependent dielectric constant of the material of NPs and the structure of the layer), EMT has its clear limitations. It is not accurate for large and very densely packed particles, as the dipolar approximation will break down. Furthermore, it is not applicable for lattice constants comparable to the wavelength of light, because there the continuum film approximation fails. Systematic comparison between effective medium theory and numerical simulations show that EMT works very well within the reasonable range of system parameters (and is qualitatively correct beyond it).

When NPs are small, the reflection is unsubstantial with only a few % reflection (*cf.* the upper panel of Fig. 12). This is not surprising as there is an insufficient amount of electrons to contribute to the oscillator strength of the localized plasmons. The other message from these graphs is the continuous shift of the reflection maxima to red when the distance between NPs gets smaller, which is a collective effect – the result of interaction between localized plasmon oscillations in each individual NP.

The optical response can be further tuned by changing the morphology of the NPs and the phase of the interface. For example, Fig. 13 shows the calculated reflectivity for SiO_2/Au core shell NPs at a solid ITO interface.[37] Thinning the shell and keeping the outer radius constant shift the plasmon resonance to blue and at the same time changes the maximum reflectivity. Furthermore as can be seen, FDTD calculations qualitatively agree very well with EMT.

Experimentally, Girault's group were the first to measure the reflectivity from such layers,[21] with trends qualitatively agreeing with theory.[36] The reflectivity of Au NP films, prepared with varying interfacial coverage and size, was measured as a function of light's incident angle, wavelength, and polarization.[21] This group added Au NPs to the interface with a micropipette, assumingly increasing the interface coverage, in order to study

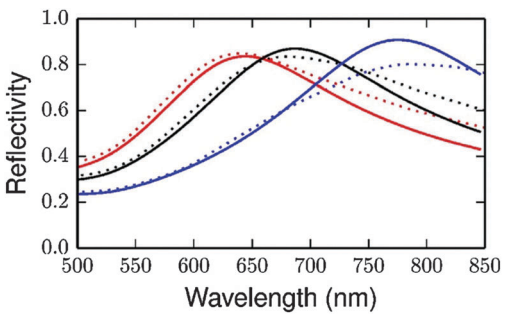

Fig. 13 Calculated reflectivity of an array of core–shell [SiO_2@Au] NPs assembled in water at a semi-infinite ITO electrode covered by a SAM spacer. Compared are the spectra calculated with the Effective Medium Dipole Approximation theory (solid lines) and finite difference time domain numerical simulations (dotted lines). The optical dielectric constant of water is 1.78; for simplicity the same value is assumed for the spacer. In the results shown, the centres of NPs are aligned in a hexagonal array (at surface coverage Γ = 0.722) in the plane disposed at a distance h = 18 nm from the surface of the ITO electrode. The outer radius of NPs, R_s = 16 nm, the optical dielectric constant of silica is taken as 2.25, and the frequency dependent dielectric permittivities of gold and ITO are fitted to the literature data. Light incidence is from water, normal to the interface. The plot shows the effect of varying shell thickness: R_c = 4 nm (blue), 6 nm (black), and 8 nm (red). This figure has been reproduced from ref. 37 with permission from the American Chemical Society.

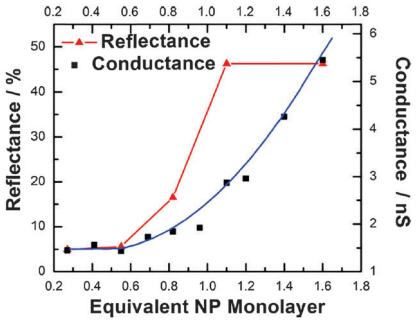

Fig. 14 The effect of the coverage of the interface with gold NPs on the reflectivity of the liquid mirror. The data correspond to varying the total amount of NPs in solution capable of covering the indicated portions of the monolayer. Comparison of the experimentally observed maximum reflectivity and the measured electrical conductance of Au NP films consisting of 60 nm Au NPs with varying surface coverage at the [heptane plus DCE]/water interface. Electrical conductance provides additional information on the properties of the film of NPs. For discussion see the text. This figure has been reproduced from ref. 21 with permission from the American Chemical Society.

its effect on the reflectance. Doing it for the incidence angles below the critical angle, θ_c, (the angle of incidence above which total reflection occurs) they observed the increase of reflection with the expected increase in the coverage. For the angles $\theta > \theta_c$, the reflectance seemed to decrease with the coverage increase since the presence of nanoparticles violates the total reflection conditions. For $\theta < \theta_c$, upon reaching the surface coverage corresponding to approximately one monolayer of Au NPs, the reflectance reached a maximum value, with the interfacial layer of NPs clearly forming a mirror visible by the naked eye. They also measured electrical conductance of the Au NP film at the interface in order to get additional insight into the structure and connectivity of the film (*cf.* Fig. 14).

In order to interpret the data in Fig. 14, we need to understand the mechanism of the electronic conductivity, *i.e.* electron transfer between the NPs. For ligand coated NPs, the transport of electrons can be substantial only when the ligands touch each other. Consider first the case of a small amount of NPs sufficient only for a submonolayer film. If NPs in the film interact with each other only through repulsive forces (*i.e.* Coulomb repulsion of charged ligands is much stronger than their van der Waals attraction), the NPs will tend to distribute equally over the surface at as large as possible distances. Adding more NPs will decrease the inter-NP separations, in order to accommodate more NPs at the interface. At distances when they start touching each other, the conductivity will start growing. If the electrostatic repulsion between NPs cannot completely dominate the van der Waals forces, there will be a minimum in the pair interaction. Under such circumstances, NPs will form two-dimensional clusters at the interface, with roughly the same interparticle distances within each cluster. Adding more NPs will cause growth of the clusters up to a percolation point at which a continuous path for electron transport along the layer emerges. Starting with this coverage the conductivity will grow. For both scenarios, above the full monolayer coverage the conductivity will continue growing as there will be new out-of-plane pathways for electron transport.

This behaviour is consistent with the results of reflectance measurements in Fig. 14, showing an increase of reflection with the increase of the NP coverage up to the full monolayer (in accordance with the general trends predicted by the theory, *cf.* Fig. 12).

The authors of ref. 21, actually, suggest that the observed absence of discernible changes in reflectance with increasing amounts of NPs (and the stabilization of the reflectance signal) indicates the formation of a homogeneous, compact mirror-like structure. Following the pioneering work of Yogev and Efrima[40] this has been dubbed MELLF (metal liquid-like film). In the case of NP-layer, this would be a very thin MELLF, as Efrima has dealt with much thicker films. The key parameter in the study of ref. 21 was the size of the Au NP. The maximum reflectance has been observed with 60 nm Au NPs, while a further increase of the NP size to 100 nm led to a decrease of the signal. The observed effects have been ascribed to an interplay between Au NP absorption, scattering and the angular dependent underlying reflectivity of the interface, and have been modelled using three-dimensional FDTD calculations.

As predicted by theory,[36,37] the control of NP surface coverage, *i.e.* the average distance between the NPs, is crucial for tuning the light reflectance from such interfaces. In a similar manner to the work performed by Girault's group,[21] this has also been achieved by direct tuning of the amount of NPs injected onto the interface. For example, Turek *et al.*[20] characterized the spectral properties of NPs adsorbed by controlling the repulsion between the NPs, through tuning the pH and electrolyte concentration in the aqueous phase. The designed 'plasmon-ruler' was calibrated by correlating the LSPR maximum of the localized surface plasmon resonance with the surface-to-surface spacing of the NPs. In this respect the correlation between *in situ* X-ray diffraction patterns and the plasmon ruler obtained at the same time on the same samples and in the same optical cell would be decisive.

New metamaterials: NP-layer-on-mirror constructs

Complementing the work on LLIs and SLIs has been the development of platforms based on the deposition of monolayers of NPs on metallic substrates typically with a nanoscale dielectric spacer.[41,42] The motivation in doing so is that such platforms can act as metamaterial absorbers as has been shown for nanocubes randomly deposited on a Au surface separated by a polymer sheet.[41] The results show that the film-coupled nanocubes provide a reflectance spectrum that can be modified by varying the geometry (the size of the cubes and/or the thickness of the spacer). Optically, each nanocube performs as a "ground patch antenna", with a nearly identical local field structure that is modified by the dielectric (plasmonic) response of the substrate metal. In such a system, a broad

range of frequencies can be addressed with an anomalously large absorption efficiency that can be attributed to an interferometric effect.

A similar approach has been used to design NP-layer-on-mirror constructs and has been investigated both theoretically and experimentally.[42] The precise structural details of the metallic nanogaps inside the optical antennae were found to dramatically modify the system plasmonic response, and is attributed to a ''complex ladder of electromagnetic modes''. Two sets of identified modes were highlighted: (i) small-facet-nanogap-related longitudinal antenna modes, and (ii) confined transverse cavity modes. These modes hybridize, subject to the morphology of the construct. The authors suggest that the richness of the optics of NP-on-mirror structures may be utilized in various emerging photochemical and optoelectronic processes.

In ref. 36, one of the examples of applications of the effective medium theory was just the light reflection from the NP-array on a metal substrate separated by an insulating spacer. The calculated reflectivity spectra of such systems have been shown to display peculiar features depending on the size of NPs, the distance between them, and the thickness of the spacer. Such theory may not reveal fine details of cavity and gap modes, but it might still capture some qualitative features of the system behaviour; tested by electrodynamic numerical simulations it could be a useful tool for the navigation of pertinent experiments.

There are clear scenarios of how the principles of such systems could be realised in electrochemical systems, with the voltage control of the structure of the layer, creating a 'third' type of electrochemical plasmonic metamaterial.

Optical visualization of nanoparticles

There is another branch of research in nanoplasmonics, which lies somewhat outside the main topic of this review, however is still worth briefly mentioning. It is driven by the demands of being able to detect and quantify NPs which can adversely affect human health as a result of ingestion, or inhalation. Although challenging, recently there has been a drive to better understand the toxicity levels as well as better understand the interaction between NPs and health. In the laboratory, when NPs are adsorbed at the interface, they can easily be visualized using techniques such as scanning probe microscopies such as AFM, SPM and STM. However when the NPs are weakly bound such methods prove to be challenging to use, due to the motion of the NPs being generated by the tips.

To circumvent such limitations, it was recently suggested that it would be possible to visualise small NPs in real time, using the effect of diffraction of surface plasmons from the presence of NPs in the vicinity of metallic films.[43] Later the same concept was used for the visualisation of DNA molecules and viruses.[44,45] Conceptually the working principle is simple: use the Kretschmann geometry, shining a laser beam on a metallic film through a prism at an angle and frequency that will excite surface plasmons in the film. That condition will depend on the medium to which the other side of the film is exposed ('environment'), *e.g.* aqueous solution or air. When satisfied, such a condition will provide a dip in reflection (the so called Attenuated Total Reflection, ATR), because some of the energy of the incident light will be expended on the excitation of the propagating surface plasmon. If an object is positioned at the interface of the film and the environment, whose optical characteristics are different from the environment, the surface plasmon wave will get diffracted from it. To put it simply, the ATR condition will locally break down, reflection will be higher and the object will be seen as a bright spot, as long as the optical contrast between the object and the environment is large enough. This is obvious for a large object, but will it be valid for NPs 20–200 nm in size? The diffraction is naturally weaker, the smaller the NP and the farther away the object is from the interface; when the NP moves away from the interface, the brightness of the image fades.

Whereas the idea is straightforward, the theory of this effect is rather complex, however, it has recently been developed in a fully analytical format, rationalizing the properties of a plasmonic image from sub-wavelength to macroscopic NPs.[46] As there are differences in refraction indices of the materials of different NPs – be they metal NPs, quantum dots, polystyrene, or gas bubbles in water, one can even distinguish from those images the class of particles we may deal with, although the exact detection of their chemical nature is hardly possible. Thus obtained videos of moving particles near interface disappearing when they move away from the interface but reappearing when getting back have recently been recorded in a device which was built by consortium, led by V. Mirsky and A. Zybin. The device demonstrates the power of plasmonic visualization of NPs, coming from air or dissolved from liquids, which themselves may be plasmonic or dielectric.

Concluding remarks

The use of the self-assembled Nanoplasmonic platforms at liquid|liquid interfaces has matured to the level of building the laboratory prototypes. Future ITIES electrochemical configuration will allow fine tuning of the position of NPs relative to the interface, with an opportunity to move NPs closer to the organic phase, and thereby amplifying the signal of analytes that prefer to dissolve in the oil phase rather than water.

It remains to be seen why the SERS signal is not so strong for spontaneously adsorbed NP arrays at the TCF electrode interface, as preliminary experiments have shown. No characterization of those structures has been made, and we do not know whether this is because we have too many or too few NPs at the interface. Electrochemical control of their population combined with X-ray diffraction and small angle reflectivity, all *in situ*, will be the major step forward, both for mirrors and sensors. A principle problem with the electrovariable mirror is that sufficiently large NPs are needed, say 40 nm in diameter. Will such NPs eagerly leave the interface, attracted to it by capillary forces in the case of ITIES, or van der Waals forces in the case of the TCF electrode/aqueous electrolyte interface?

Estimates exist but due to the complexity of the system they are not very reliable. The way out for the liquid–liquid interface would be to reduce surface tension, adding surfactants. Something to try for the TCF electrode is to cover it by a SAM and thereby increase its electrochemical window, which might allow us to apply larger voltage.

Will larger NPs have higher propensity to agglomerate, instead of forming a monolayer? Van der Waals forces scale with the volume of NPs whereas the surface charge with the surface area. A lot more studies should be done in this direction.

Much can be achieved playing with the shapes of nanoparticles, at least for sensor applications. One can easily prepare spheres or pyramids, needles or ellipsoids, or origami type of hierarchical structures[47] (scaffolding NPs of different sizes with the DNA), and trying to build hierarchical structures with Stockman-like antennae,[48] which is expected to dramatically amplify the hot spots. All these opportunities should be explored to further increase the sensitivity of the sensor. At a first glance it looks that it is sensitive enough, but having in mind in-the-field application in a noisy, dusty environment, any sensitivity enhancement would be welcome! It is not excluded that doing that practically important work, one might eventually discover new opportunities that may be offered by these fascinating self-building optical metamaterials.

Of course there are many other applications that can be envisaged using an ITIES that has not been discussed in this article. For example, ITIES with metallic NPs adsorbed can be used for electrocatalysis.[49] Although practical applications of such systems may be limited, as industrial scale systems require huge, 'volume filling' reaction space, from the fundamental point of view such systems open new horizons for investigation and understanding of the elementary act of electrochemical reactions. In the latest paper by Girault's group,[50] which used 12 and 38 nm Au NPs, a precise control of the Galvani potential difference between the two phases and the potential-controlled variation of Fermi-levels in NPs has been achieved. This resulted in direct control of the rate and the direction of electron transfer at a floating gold nanofilm.

Acknowledgements

The authors are thankful to Jeremy Baumberg, Ilan Benjamin, Angela Demetriadou, Hubert Girault, Vladimir Mirsky, Steve Roser, Mark Schlossman, Debabrata Sikdar, and James Wilton-Ely for useful discussions. AAK, JBE and ARK are thankful to the EPSRC grant (EP/L02098X/1) for the support of this research. AAK also thanks EU FP7 grant Nanodetector project NMP.211.1.3-1 for partial support. JBE also acknowledges support of an ERC starting investigator grant, and MU of the Israel Science foundation.

References

1 H. H. Girault and D. H. Schiffrin, in *Electroanalytical Chemistry*, ed. A. J. Bard, Marcel Dekker, New York, 1989, vol. 15, p. 1.
2 G. M. Luo, S. Malkova, J. Yoon, D. G. Schultz, B. H. B. H. Lin, M. Meron, I. Benjamin, P. Vanysek and M. L. Schlossman, *Science*, 2006, **311**, 216–218.
3 D. Michael and I. Benjamin, *J. Electroanal. Chem.*, 1998, **450**, 335–345.
4 N. E. A. Cousens and A. R. Kucernak, *Electrochem. Commun.*, 2011, **13**, 1539–1541.
5 V. A. Parsegian, *Van der Waals forces*, Cambridge University Press, Cambridge, 2006.
6 R. A. Sperling and W. J. Parak, *Philos. Trans. R. Soc., A*, 2010, **368**, 1333–1383.
7 M. E. Flatté, A. A. Kornyshev and M. Urbakh, *J. Phys.: Condens. Matter*, 2008, **20**, 073102.
8 M. E. Flatte, A. A. Kornyshev and M. Urbakh, *J. Phys. Chem. C*, 2010, **114**, 1735–1747.
9 M. A. Vorotyntsev, in *Solvation and interionic interactions at the metal-electrolyte interface, in the Chemical Physics of Solvation*, ed. R. R. Dogonadze, E. Kalman, A. A. Kornyshev and J. Ulstrup, 1988, Part C, pp. 401–432.
10 D. Wang, R. Hu, M. J. Skaug and D. K. Schwartz, *J. Phys. Chem. Lett.*, 2015, **6**, 54–59.
11 L. L. Dai, R. Sharma and C. Y. Wu, *Langmuir*, 2005, **21**, 2641–2643.
12 L. Isa, F. Lucas, R. Wepf and E. Reimhult, *Nat. Commun.*, 2011, **2**, 438.
13 M. K. Sanyal, V. V. Agrawal, M. K. Bera, K. P. Kalyanikutty, J. Daillant, C. Blot, S. Kubowicz, O. Konovalov and C. N. R. Rao, *J. Phys. Chem. C*, 2008, **112**, 1739–1743.
14 S. Kubowicz, M. A. Hartmann, J. Daillant, M. K. Sanyal, V. V. Agrawal, C. Blot, O. Konovalov and H. Moehwald, *Langmuir*, 2009, **25**, 952–958.
15 J. M. Perera and G. W. Stevens, *Anal. Bioanal. Chem.*, 2009, **395**, 1019–1032.
16 M. P. Cecchini, V. A. Turek, J. Paget, A. A. Kornyshev and J. B. Edel, *Nat. Mater.*, 2013, **12**, 165–171.
17 K. Kim, H. S. Han, I. Choi, C. Lee, S.-G. Hong, S. H. Sue, L. P. Lee and T. Kang, *Nat. Commun.*, 2013, **6**, 6321.
18 P. Galletto, H. H. Girault, C. Gomis-Bas, D. J. Schiffrin, R. Antoine, M. Broyer and P. F. Brevet, *J. Phys.: Condens. Matter*, 2007, **19**, 375108.
19 N. Younan, M. Hojeij, L. Ribeaucourt and H. H. Girault, *Electrochem. Commun.*, 2010, **12**, 912–915.
20 V. A. Turek, M. P. Cecchini, J. Paget, A. R. Kucernak, A. A. Kornyshev and J. B. Edel, *ACS Nano*, 2012, **9**, 7789–7799.
21 P. P. Fang, S. Chen, H. Deng, M. D. Scanlon, F. Gumy, H. J. Lee, D. Momotenko, V. Amstutz, F. Cortés-Salazar, C. M. Pereira, Z. L. Yang and H. H. Girault, *ACS Nano*, 2013, **7**, 9241–9248.
22 M. Angel Fernandez-Rodriguez, J. Ramos, L. Isa, M. Angel Rodriguez-Valverde, M. Angel Cabrerizo-Vilchez and R. Hidalgo-Alvarez, *Langmuir*, 2015, **31**, 8818–8823.
23 S. Kinge, M. Crego-Calama and D. N. Reinhoudt, *ChemPhysChem*, 2008, **9**, 20–42.
24 A. Boker, J. He, T. Emrick and T. P. Russell, *Soft Matter*, 2007, **3**, 1231–1248.

25 M. K. Bera, H. Chan, D. F. Moyano, H. Yu, S. Tatur, D. Amoanu, W. Bu, V. M. Rotello, M. Meron, P. Kral, B. Lin and M. L. Schlossman, *Nano Lett.*, 2014, **14**, 6816–6822.
26 N. Laanait, M. Mihaylov, B. Hou, H. Yu, P. Vanýsek, M. Meron, B. Lin, I. Benjamin and M. L. Schlossman, *Proc. Natl. Acad. Sci. U. S. A.*, 2012, **109**, 20326–20331.
27 Y. Cheng and D. J. Schiffrin, *J. Chem. Soc., Faraday Trans.*, 1996, **92**, 3865–3871.
28 B. Su, J. P. Abid, D. J. Fermin, H. H. Girault, H. Hoffmannova, P. Krtil and Z. Samec, *J. Am. Chem. Soc.*, 2004, **126**, 915.
29 M. Marinescu, M. Urbakh and A. A. Kornyshev, *Phys. Chem. Chem. Phys.*, 2012, **14**, 1371.
30 C. Sönnichsen, B. M. Reinhard, J. Liphardt and A. P. Alivisatos, *Nat. Biotechnol.*, 2005, **23**(6), 741–745.
31 Y. Levin, *Rep. Prog. Phys.*, 2002, **65**, 1577–1632.
32 S. G. Booth, D. P. Cowcher, R. Goodacre and R. A. W. Dryfe, *Chem. Commun.*, 2014, **50**, 4482–4484.
33 P. S. Toth, Q. M. Ramasse, M. Velicky and R. A. W. Dryfe, *Chem. Sci.*, 2015, **6**, 1316–1323.
34 M. P. Cecchini, V. A. Turek, A. Demetriadou, G. Britovsek, T. Welton, A. A. Kornyshev, D. E. T. Wilton-Ely and J. B. Edel, *Adv. Opt. Mater.*, 2014, **2**, 966–977.
35 K. Kneipp, M. Moskovits and H. Kneipp, *Surface-enhanced Raman scattering: physics and applications*, Springer, 2006, vol. 103.
36 A. A. Kornyshev, M. Marinescu, J. Paget and M. Urbakh, *Phys. Chem. Chem. Phys.*, 2012, **14**, 1850–1859.
37 J. Paget, V. Walpole, M. B. Jorquera, J. B. Edel, M. Urbakh, A. A. Kornyshev and A. Demetriadou, *J. Phys. Chem. C*, 2014, **118**, 23264–23273.
38 N. J. Halas, S. Lal, W.-S. Chang, S. Link and P. Nordlander, *Chem. Rev.*, 2011, **111**, 3913–3961.
39 A. Liebsch and B. N. J. Persson, *J. Phys. C: Solid State Phys.*, 1983, **16**, 5375.
40 D. Yogev and S. Efrima, *J. Phys. Chem.*, 1988, **92**, 5754–5760.
41 A. Moreau, C. Ciracì, J. J. Mock, R. T. Hill, Q. Wang, B. J. Wiley, A. Chilkoti and D. R. Smith, *Nature*, 2012, **492**, 86–90.
42 C. Tserkezis, R. Esteban, D. O. Sigle, J. Mertens, L. O. Herrmann, J. J. Baumberg and J. Aizpurua, *Phys. Rev. A: At., Mol., Opt. Phys.*, 2015, **92**, 053811.
43 A. Zybin, Y. A. Kuritsyn, E. L. Gurevich, V. V. Temchura, K. Uberlaand and K. Niemax, *Plasmonics*, 2010, **5**, 31–35.
44 A. R. Halpern, J. B. Wood, Y. Wang and R. M. Corn, *ACS Nano*, 2014, **8**, 1022–1030.
45 S. Wang, X. Shan, U. Patel, X. Huang, J. Lu, J. Li and N. Tao, *Proc. Natl. Acad. Sci. U. S. A.*, 2010, **107**, 16028–16032.
46 A. Demetriadou and A. A. Kornyshev, *New J. Phys.*, 2015, **17**, 013041.
47 T. Pellegrino, S. Kudera, T. Liedl, A. Muñoz Javier, L. Manna and W. J. Parak, *Small*, 2005, **1**, 48–63.
48 L. Kuiru, M. I. Stockman and D. J. Bergman, *Phys. Rev. Lett.*, 2003, **91**, 227402.
49 A. Trojanek, J. Langmaier and Z. Samec, *Electrochem. Commun.*, 2006, **8**, 475–481.
50 E. Smirnov, P. Peljo, M. D. Scanlon and H. Girault, *ACS Nano*, 2015, **9**, 6565–6575.

